



**TECHNISCHE  
UNIVERSITÄT  
DRESDEN**



**8IMC\_223**

Observation of the failure mechanism of  
brick masonry doublets with cement and lime  
mortars by microfocus X-ray computed  
tomography

HENDRICKX R.; BRUYNINCKX K.;  
SCHUEREMANS L.; KERCKHOFS G.;  
VERSTRYNGE E.; WEVERS M.;  
VAN BALEN K.

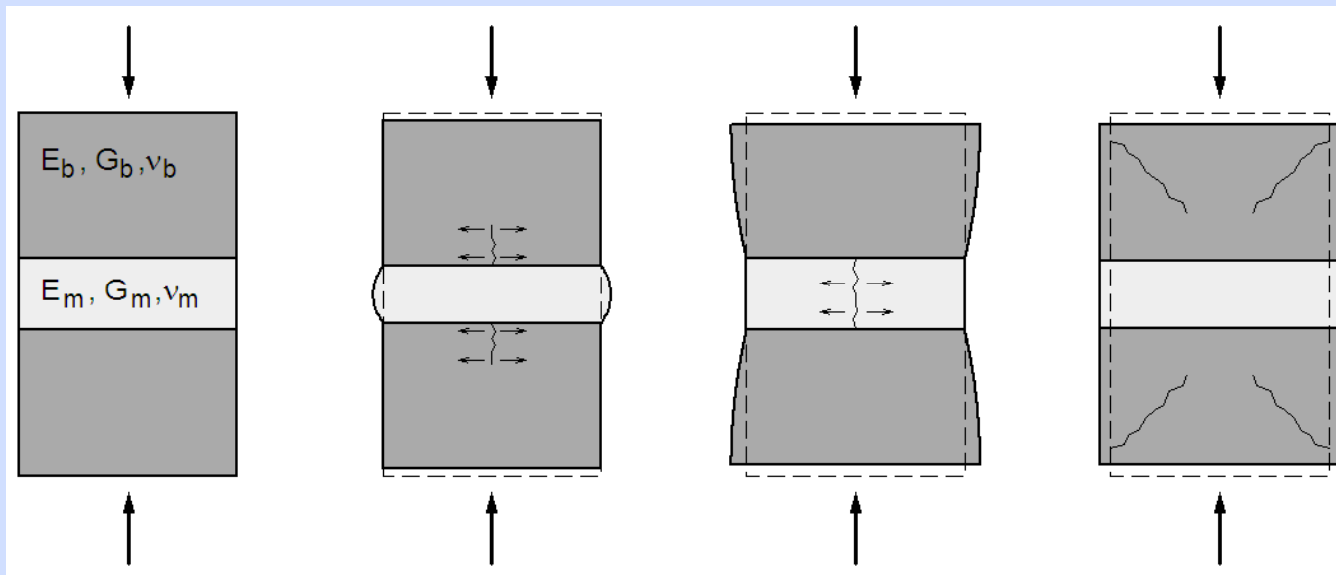
July 5th, 2010 at Hilton Hotel

# Introduction: failure modes of masonry

Uniaxial compression leads to failure of mode I, i.e. formation of internal shear planes due to tensile cracking (Lourenço 1996).

Different failure modes according to Hilsdorf 1969:

- if the brick's stiffness is higher than the mortar's stiffness, the mortar will tend to expand more laterally, which causes tensile stress in the brick;
- if the mortar's stiffness is higher than the brick's stiffness, the brick will tend to expand more laterally, which causes tensile stress in the mortar;
- if stiffnesses are comparable, a homogeneous behaviour is expected, with typically the formation of conical shear planes.



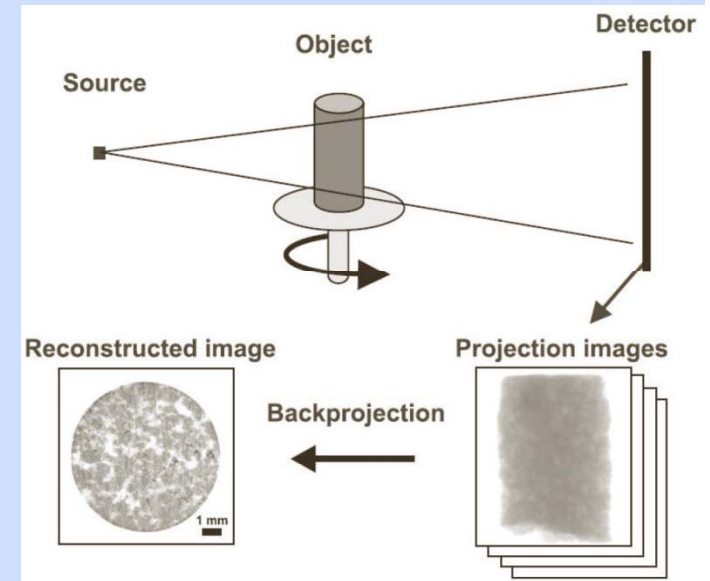
# Introduction: failure of mortar

Dependent on the ratio between horizontal and vertical stresses  
(Hayen 2004)

- Stress coefficient  $\kappa$ : 
$$\kappa = \frac{\sigma_{vert}}{\sigma_{hor}}$$
- for  $\kappa < 0.25$  the tensile-shear mechanism is dominant
- for  $\kappa > 0.25$  the pore collapse mechanism was dominant

# Introduction: microfocus computed tomography (CT) combined with compression

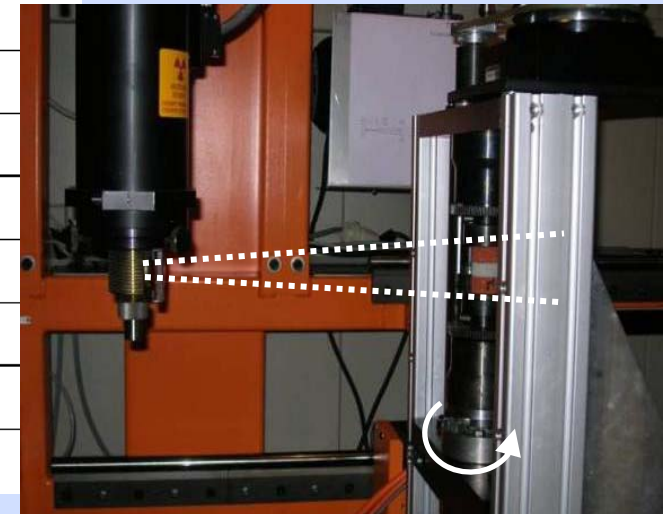
- Cylindrical object placed between source and detector
- Images taken every rotation step of  $1^\circ$ , over  $180^\circ$
- Reconstruction of horizontal slices from the raw data.



size (m)	brick	mortar	visualisation technique
$10^{-9}$		gel pores	
$10^{-6}$	pores	cap. pores / micro-cracks	
	pores	binder particles	
		air bubbles	
$10^{-3}$	inclusions	sand grains	
	constr. element	constr. element	

Visualisation techniques are indicated by arrows on the right side of the table:

- $\mu$ CT (micro-CT) covers the range from approximately  $10^{-6}$  m to  $10^{-3}$  m.
- synchrotron CT covers the range from approximately  $10^{-6}$  m to  $10^{-3}$  m.
- nanoCT covers the range from approximately  $10^{-9}$  m to  $10^{-6}$  m.



# Materials

## The brick: “Spaans Rood” by Wienerberger

- compressive strength 10.2 MPa on cylinders, 8.9 MPa on doublets (NBN B24-201)
- Young’s modulus 1095 MPa
- dynamic Young’s modulus (ultrasound propagation) 3730 MPa
- porosity 28.1%;

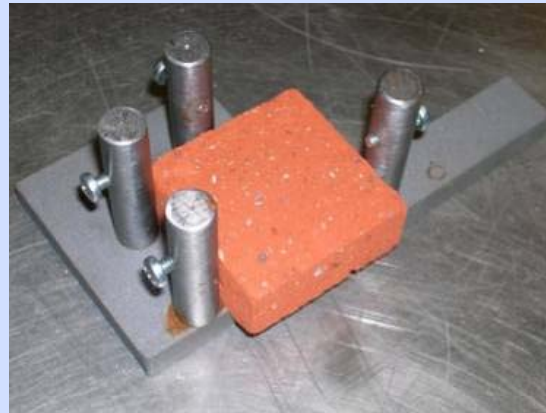
## The mortars: 5 different types were selected

	Lime hydrate un-carbonated	Lime hydrate carbonated	Hydraulic lime	Lime-cement	Cement
Composition					
Binder/sand ratio (kg/kg)	0.127	0.127	0.212	0.212	0.247
Water/binder ratio (kg/kg)	1.810	1.810	1.102	1.019	0.907
Mechanical properties					
$f_{c,m}$ (MPa)	0.81	2.22	1.37	10.88	29.48
$E_{dyn,m}$ (MPa)	3244	5449	2573	11182	21997
$\rho$ (kg/m <sup>3</sup> )	1671	1722	1861	1841	2016
$f_{t,flex,m}$ (MPa)	0.37	0.83	0.49	3.19	8.05

# Sample preparation



Accessory device



Step 1: brick bottom layer



Step 2: hybrid mortar layer



Step 3: parallel brick top layer



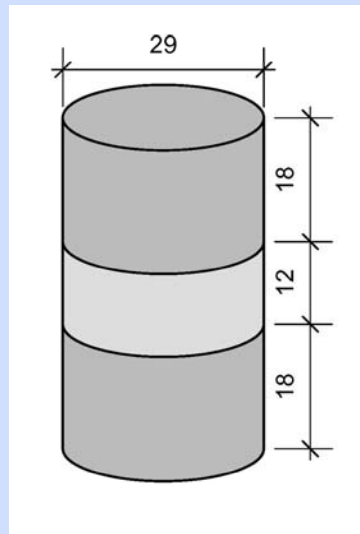
Step 4: sample before core drilling



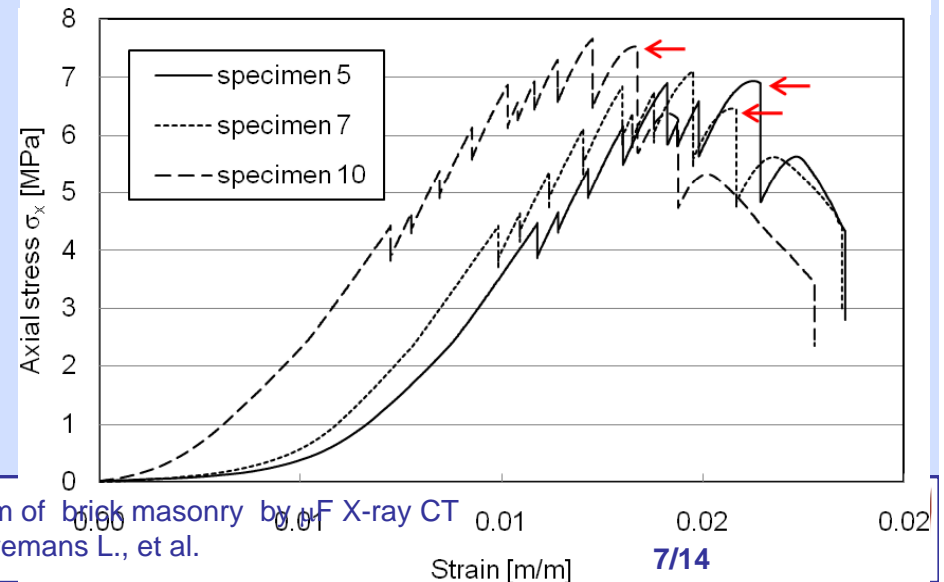
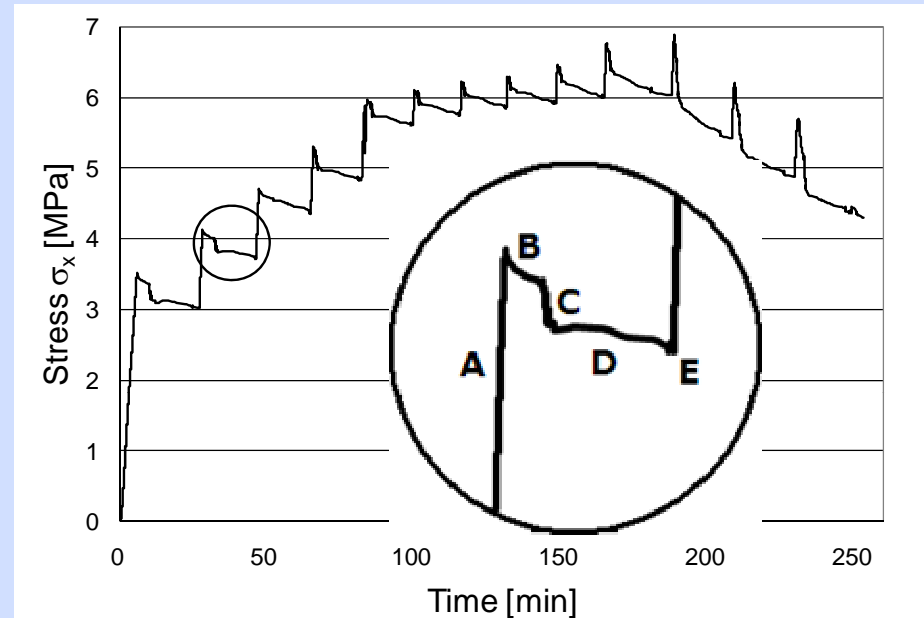
Test sample –  
d=29mm – h=48 mm

# Testing procedure

- Preliminary determination of compressive strength of specimens
- procedure in steps, rate-controlled but fixed at determined stress-levels
- each step has 5 stages
- data acquisition during stage D
- importance of relaxation after fixing the displacement during each step



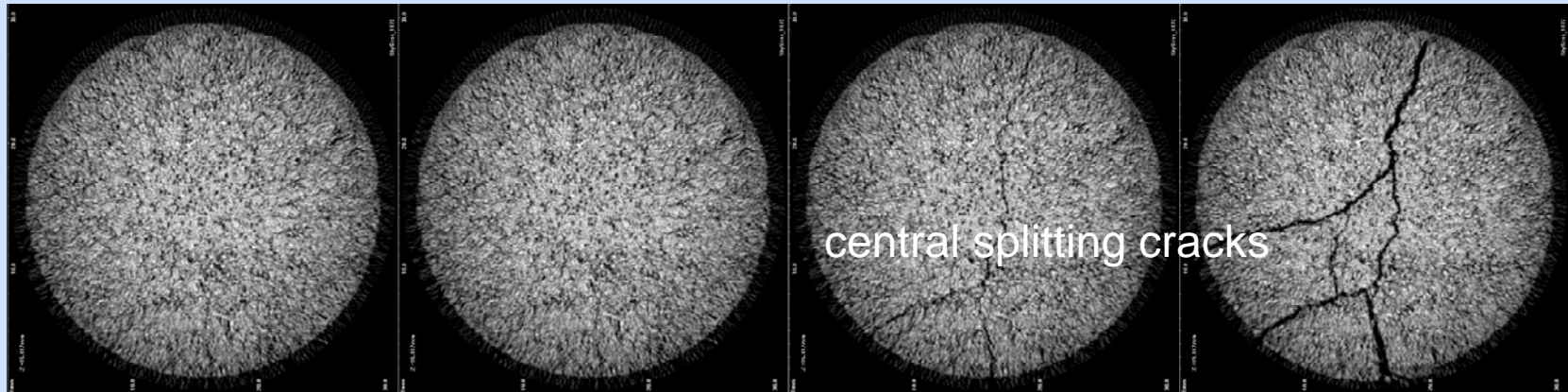
specimen geometry



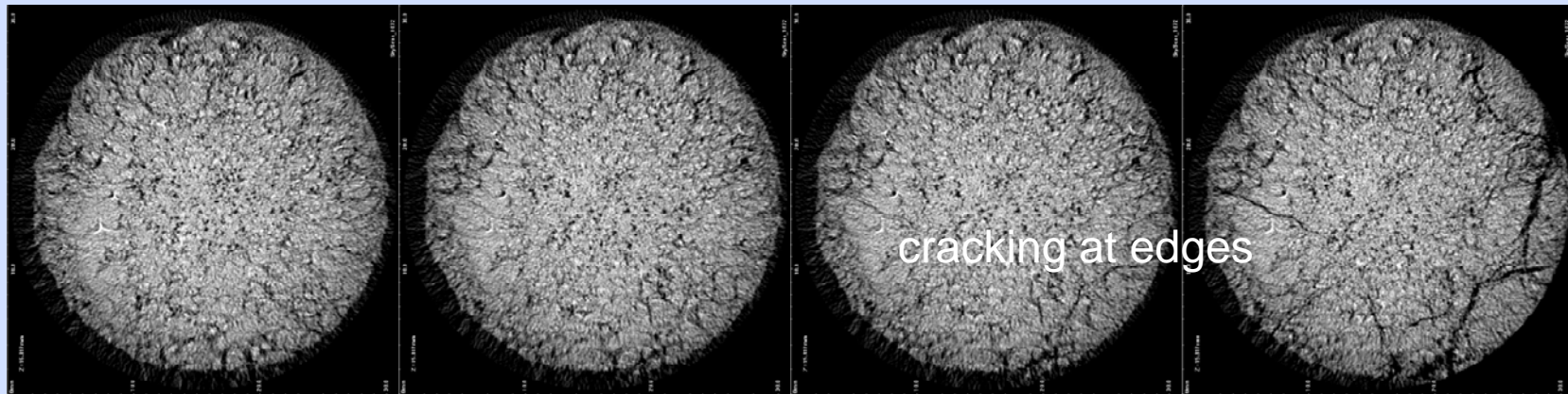


# Results and data treatment: horizontal slices

First processed data consists of horizontal slices, that can be stacked to 3D images or vertical sections



4 load steps in specimen with cement mortar: section through symmetry plane

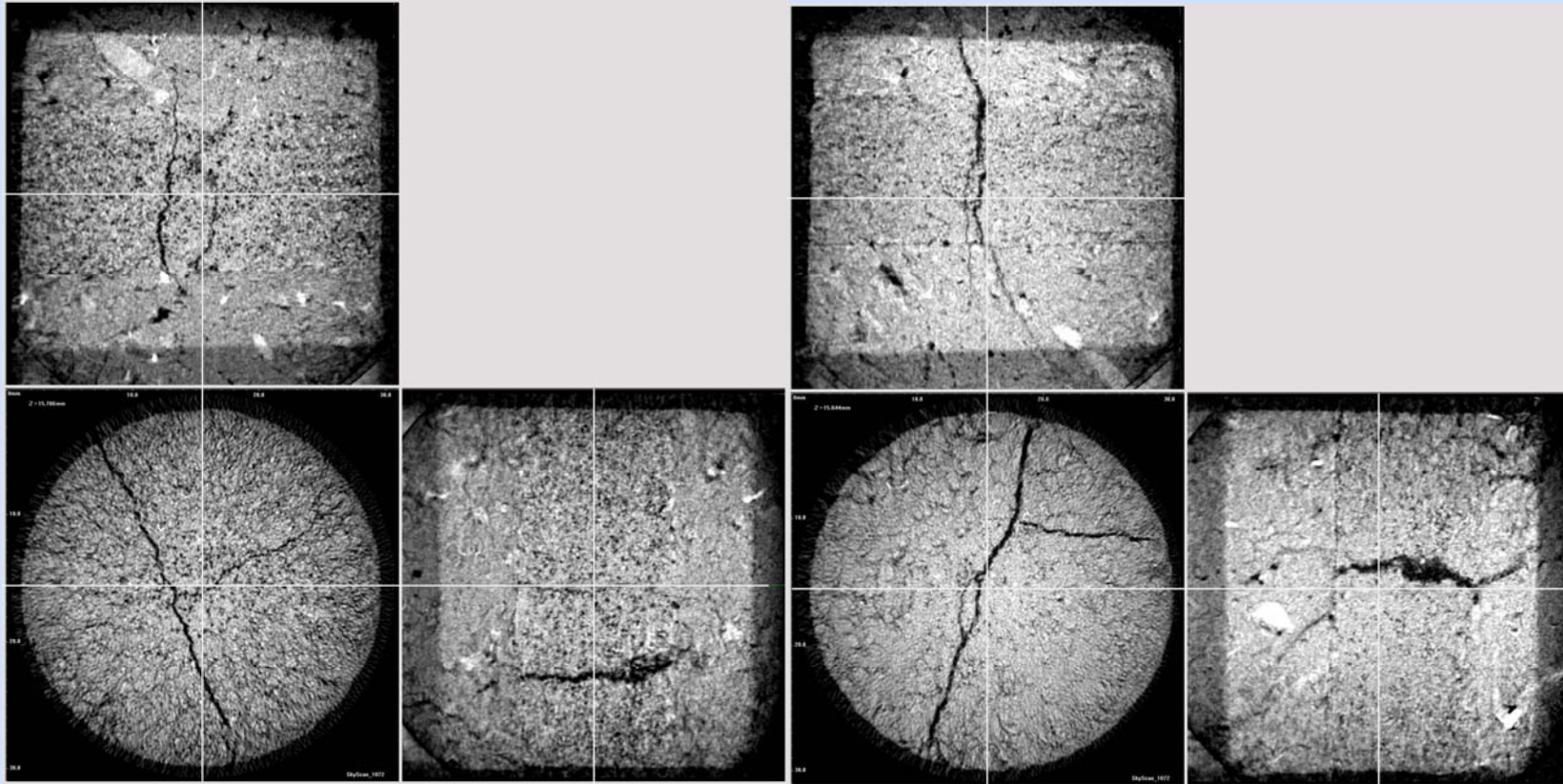


4 load steps in specimen with hydraulic lime mortar



# Results: cement mortar and lime-cement mortar

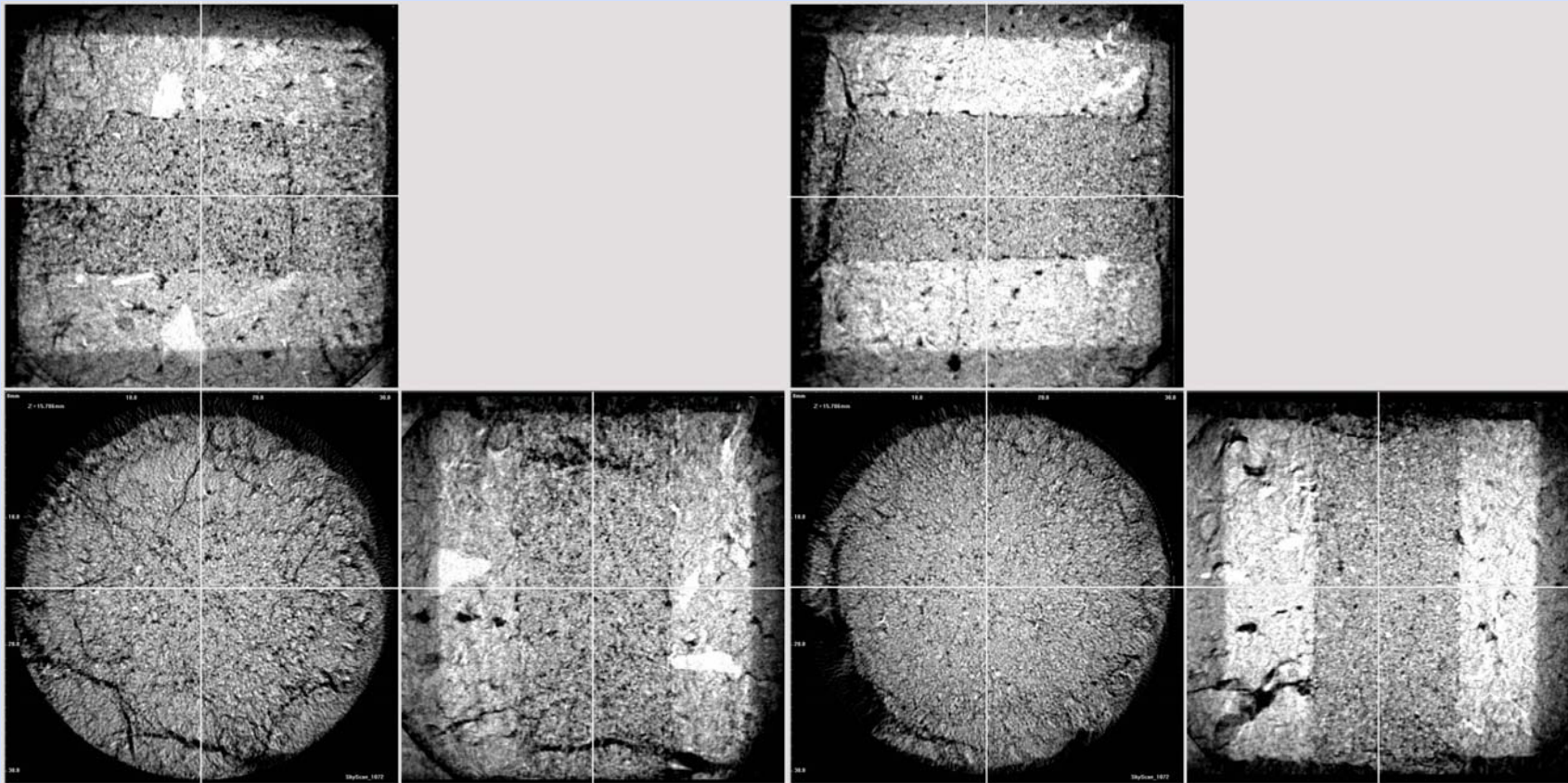
Stack of slices used to produce 3 orthogonal sections



Cement mortar specimen 7.

Lime-cement mortar specimen 6.

# Results: hydraulic lime mortar and uncarbonated lime hydrate mortar

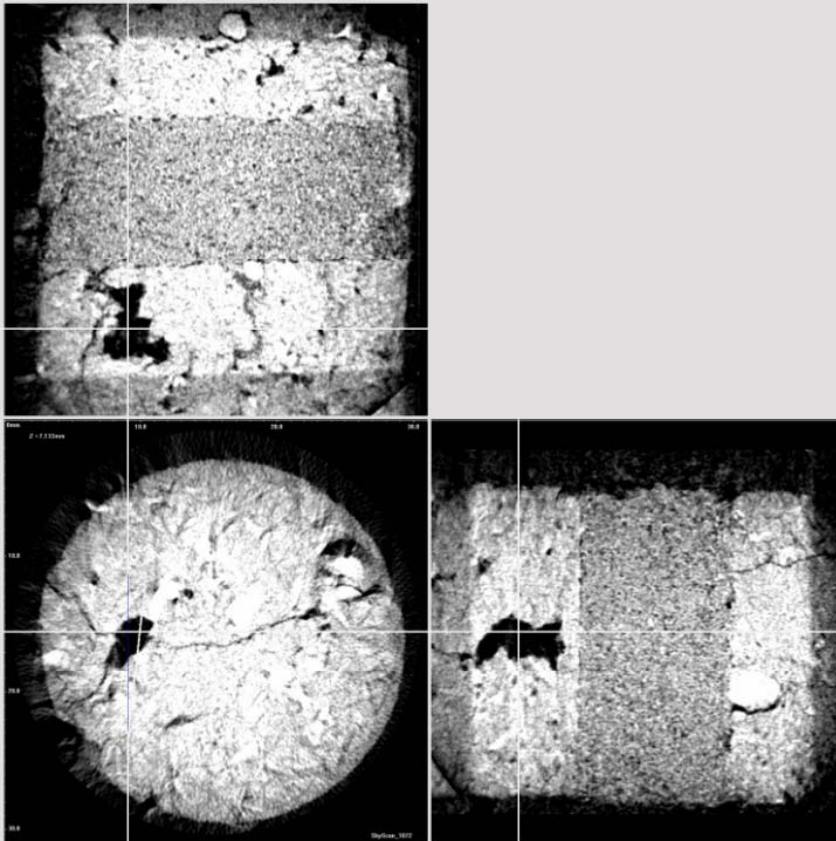


Hydraulic lime mortar specimen 7.

Uncarbonated lime hydrate mortar specimen 9.

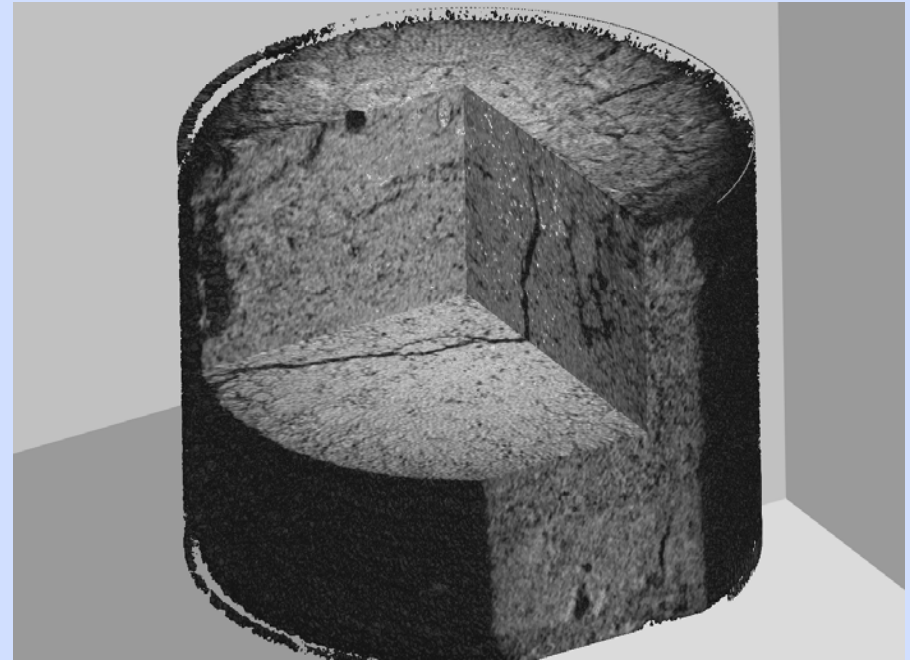


# Results: carbonated lime mortar and 3D rendering



Carbonated lime hydrate mortar specimen 3.

3D rendering of lime-cement mortar specimen 6.



# Quantitative analysis

- Can we distinguish compaction of the materials through quantitative analysis of attenuated radiation?

- Beer's law for attenuation of X-rays:  $\frac{I_t}{I_0} = \exp(-\mu d)$

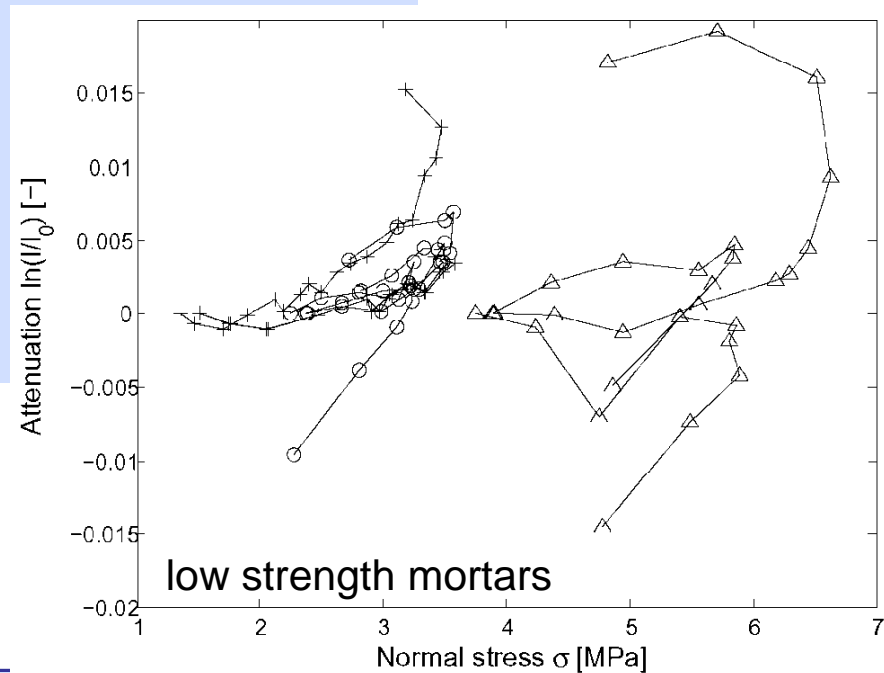
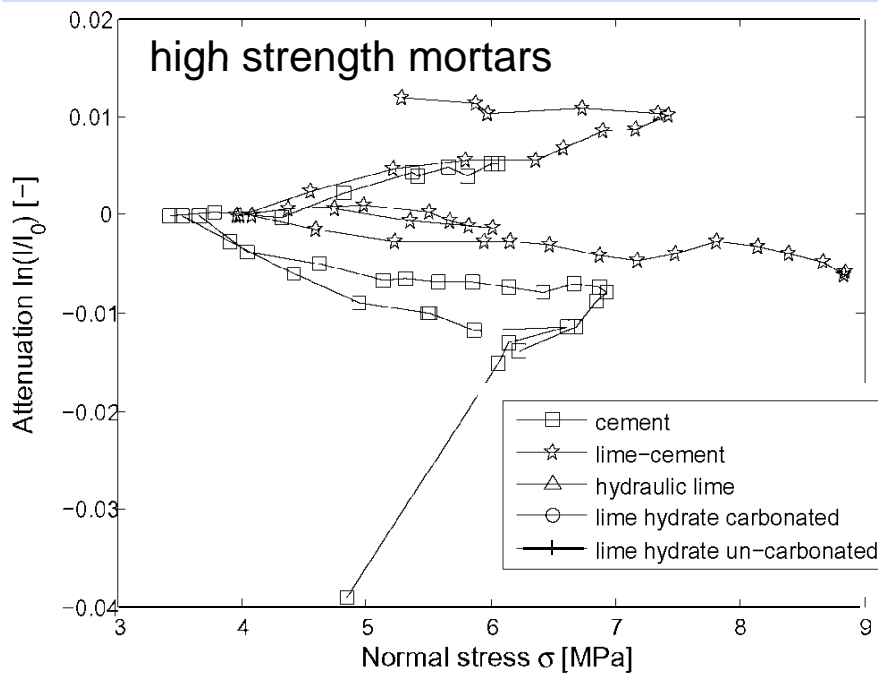
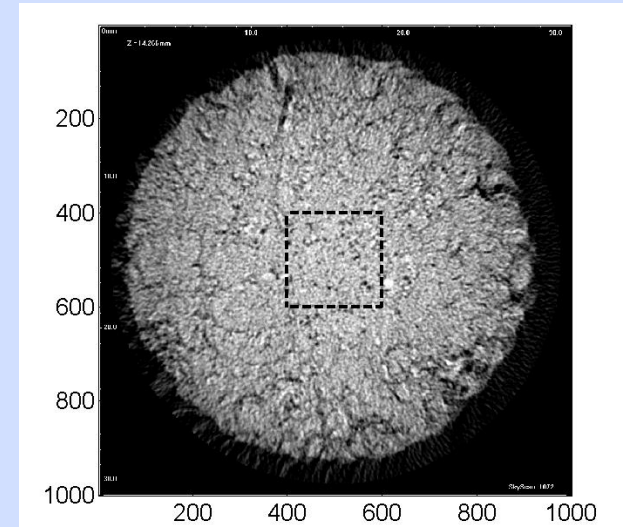
$$\mu = -\frac{1}{d} \ln\left(\frac{I_t}{I_0}\right)$$

Experimental determination of attenuation coefficients from known thickness  $d$  and incident/transmitted intensities ( $I_0$  and  $I_t$ ):

	Lime hydrate un-carbonated	Lime hydrate carbonated	Hydraulic lime	Lime-cement	Cement
$\mu_{\text{mortar}}$ [1/m]	59.1	59.1	60.0	58.3	68.9
$\mu_{\text{brick}}$ [1/m]	70.8	70.3	69.6	69.3	71.1

# Quantitative analysis

- Average value of attenuation in mortar taken from central area in the slice of the symmetry plane.
- Plotted as a function of increasing normal stress.
- Unclear evolution for the high strength mortars.
- Clear increase for uncarbonated lime mortar and hydraulic lime mortar, indicates compaction.





# Conclusions

- Technique of CT combined with loading is feasible for masonry, although labour-intensive and requiring meticulous specimen preparation.
- The resolution for micro-CT provides macro- and meso-crack information, but misses the micron-scale, which is essential for crack initiation.
- Spatial resolution can however be improved when decreasing the field of view, but then the overview of the three elements is lost.
- Observations confirm the classical hypotheses of masonry failure. The link between the observed failure and stiffness ratios was clearly established.
- Compaction of low strength mortars – assumed to occur due to pore collapse - could be quantified.